Journal of Alloys and Compounds 509 (2011) 2007–2010

Contents lists available at ScienceDirect

Journal of Alloys and Compounds

journal homepage: www.elsevier.com/locate/jallcom

Luminescence properties of novel Sm^{3+}, Dy^{3+} doped $LaMoBO_6$ phosphors

Xinmin Zhang[a], Hyo Jin Seo[b,*]

[a] School of Materials Science and Engineering, Central South University of Forestry and Technology, Changsha 410004, China
[b] Department of Physics, Pukyong National University, 599-1, Daeyeon 3-Dong, Nam-Gu, Busan 608-737, Republic of Korea

ARTICLE INFO

Article history:
Received 6 August 2010
Received in revised form 10 October 2010
Accepted 22 October 2010
Available online 3 November 2010

Keywords:
Phosphors
Solid state reactions
Optical properties
Luminescence

ABSTRACT

Luminescence properties of the Sm^{3+}, Dy^{3+} doped $LaMoBO_6$ phosphors are reported. $LaMoBO_6$:Sm^{3+} exhibits orange emission corresponding to the $^4G_{5/2} \rightarrow {}^6H_{7/2}$ transition. $LaMoBO_6$:Dy^{3+} exhibits two emission bands. The yellow band (570 nm) corresponds to the $^4F_{9/2} \rightarrow {}^6H_{13/2}$ transition, and the blue one (482 nm) corresponds to the $^4F_{9/2} \rightarrow {}^6H_{15/2}$ transition. The optimum concentration of Sm^{3+} and Dy^{3+}, the critical distance of the concentration quenching, and the decay curves have also been investigated. The analysis of the decay curves indicates that cross-relaxation is primarily responsible for the concentration quenching.

1. Introduction

Luminescence materials are important for modern technology because of their ability to convert electromagnetic radiation (i.e., UV and IR light) into visible light [1]. Recently, the development of rare earth (RE) ions activated novel luminescent materials have attracted more attention due to their potential applications in different optical display systems [2–9]. Because the 4f electrons of RE ions are shielded by the outer 5s and 5p electrons, the intra-4f emission spectra of RE ions are characterized by narrow lines with high color purity. The emission of Sm^{3+} is situated in the orange spectral region and consists of transitions from the excited $^4G_{5/2}$ level to the ground state $^6H_{5/2}$ and higher levels ^6H_J ($J > 5/2$) [10–12]. The luminescence lines of Dy^{3+} are in the 480 nm region (blue) due to the $^4F_{9/2} \rightarrow {}^6H_{15/2}$ transition, and in the 570 nm region (yellow) due to the $^4F_{9/2} \rightarrow {}^6H_{13/2}$ transition. The influence of the crystal structure on the yellow intensity is greater than that on the blue intensity. As the crystal structure is changed, the blue to yellow intensity ratio (B/Y) of Dy^{3+} emission will change [13]. The color of the luminescence is close to white if a suitable ratio of B/Y obtained. Therefore, Dy^{3+} doped materials may be potential two primary color phosphors [12,14,15].

Recently, molybdates and tungstates with scheelite structure are considered as good host lattices under near-UV or blue excitation due to their MoO_4 tetrahedron and WO_4 unit [16–20]. $LaMoBO_6$ belongs to monoclinic structure. The molybdenum atoms are trigonal bipyramidally coordinated by five oxygen atoms, forming an infinite $(MoO_4)^{2-}$ anionic chain by corner-sharing O atoms down the *b*-axis [21]. Our former investigation on $LaMoBO_6$:Eu^{3+} phosphor indicates that the Eu^{3+} site in this compound lacks inversion symmetry [4]. Su et al. reported that when Dy^{3+} is located at a site of high symmetry with an inverse center, Dy^{3+} displays no luminescence, and the B/Y of Dy^{3+} located at a site deviated from an inverse center is less than that of Dy^{3+} located at a site without an inverse center [13]. To the best of our knowledge, the luminescence properties of RE ions doped $LaMoBO_6$ phosphors have not been reported widely. In this work the photoluminescence (PL) properties of Sm^{3+} and Dy^{3+} activated $LaMoBO_6$ phosphors are presented as well as their concentration dependence.

2. Experimental

$La_{1-x}Sm_xMoBO_6$ and $La_{1-x}Dy_xMoBO_6$ phosphors were prepared according to standard solid-state technique. High-purity starting materials La_2O_3 (Aldrich, 99.9%), $(NH_4)_6Mo_7O_{24}{\cdot}4H_2O$ (Aldrich, 99.9%), H_3BO_3 (Aldrich, 99.99%, 10 mol% excess to compensate the evaporation in the heating processes), Sm_2O_3 (Aldrich, 99.99%) and Dy_2O_3 (Aldrich, 99.99%) were used. The well mixed materials were annealed at 800 °C for 12 h in air with an intermediate grinding. The structural characteristics of samples were examined from X-ray diffraction (XRD) using a Rigaku D/max 2200 Diffractometer (Rigaku Corp., Tokyo, Japan) with Cu Ka radiation at 40 kV, 30 mA. The PL emission and excitation spectra were performed at room temperature using Fluorolog-3 Fluorescence Spectrophotometer (Jobin Yvon Inc., France) with 450W Xenon lamps. The luminescence decays were measured by monitoring the given emission from the samples under 355 nm pulsed laser excitation. Decay profiles were recorded with a LeCroy 9301 digital storage oscilloscope (LeCroy Corp., NY) in which the signal was fed from PMT. The photoluminescence quantum yield was measured by a 4 Port 150 mm $BaSO_4$ coated integrating sphere which fits directly into the FSP920 (Edinburgh Instruments) sample chamber. FSP920 Time Resolved and Steady State Fluorescence Spectrometers (Edinburgh Instruments)

* Corresponding author. Tel.: +82 51 629 5568; fax: +82 51 629 5549.
E-mail addresses: zhangxinminam@yahoo.com (X. Zhang), hjseo@pknu.ac.kr (H.J. Seo).

0925-8388/$ – see front matter © 2010 Elsevier B.V. All rights reserved.
doi:10.1016/j.jallcom.2010.10.119

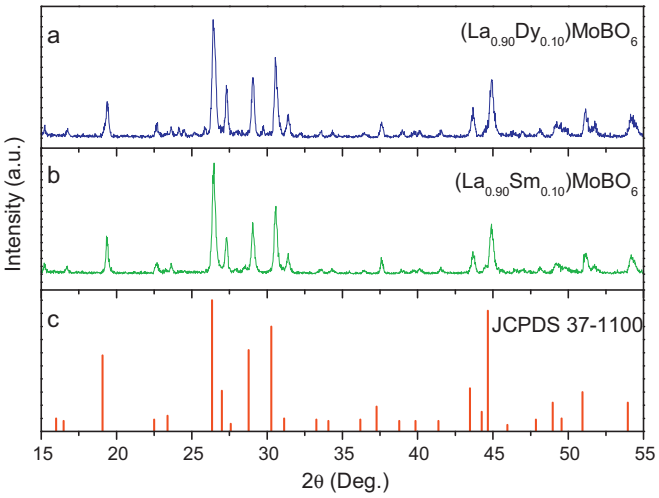

Fig. 1. XRD patterns of $La_{0.90}MoBO_6$:0.10Sm^{3+} and $La_{0.90}MoBO_6$:0.10Dy^{3+} phosphors.

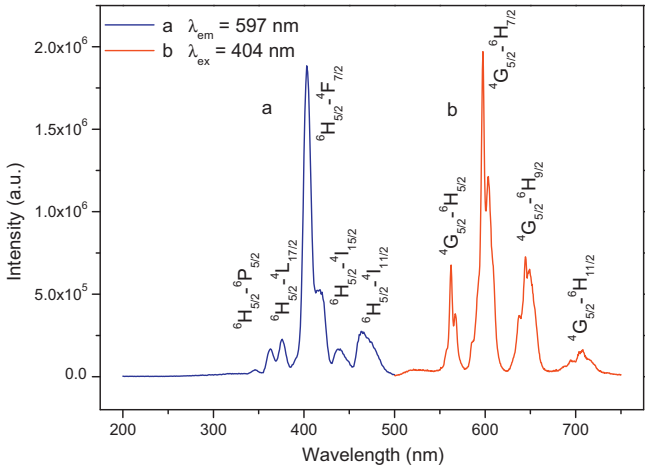

Fig. 2. PL excitation and emission spectra of $La_{0.99}MoBO_6$:0.01Sm^{3+}.

equipped with a 450 W Xe lamp, TM300 excitation monochromator and double TM300 emission monochromators and Red PMT.

3. Results and discussion

3.1. Structure characterization

The crystal structure of $LaMoBO_6$ compound has been investigated by means of single-crystal X-ray diffraction recently. $LaMoBO_6$ crystallizes in monoclinic space group $P2_1/c$ with the lattice parameters: $a = 10.2968(8)$, $b = 4.1636(3)$, and $c = 23.8587(15)$ Å [21]. The XRD patterns of $La_{0.90}Sm_{0.10}MoBO_6$ and $La_{0.90}Dy_{0.10}MoBO_6$ phosphors are shown in Fig. 1(a) and (b). All the diffraction peaks can be indexed to pure monoclinic structured $LaMoBO_6$ (JCPDS card no. 37-1100) except for some impurity phase detected in $La_{0.90}Dy_{0.10}MoBO_6$ sample. Because the electric charges of La^{3+}, Sm^{3+}, and Dy^{3+} are identical and the radii of them are close ($r_{La} = 0.127$ nm, $r_{Sm} \approx 0.113$ nm, $r_{Dy} \approx 0.108$ nm, coordination number (CN) = 10) [22], the doped Sm^{3+}, Dy^{3+} ions can substitute the La^{3+} sites easily.

3.2. Luminescence properties of $LaMoBO_6$ doped with Sm^{3+}

The PL excitation and emission spectra of $La_{0.99}Sm_{0.01}MoBO_6$ are shown in Fig. 2. The excitation bands peaking at 363, 376, 404, 439 and 465 nm are assigned to the transitions of $^6H_{5/2} \rightarrow {}^6P_{5/2}$, $^4L_{17/2}$, $^4F_{7/2}$, $^4I_{15/2}$ and $^4I_{11/2}$, respectively [15]. The $^6H_{5/2} \rightarrow {}^4F_{7/2}$ transition is the strongest excitation band. In addition, no obvious charge transfer (CT) band due to $O^{2-} \rightarrow Sm^{3+}$ or host related absorption band are observed in Fig. 1(a) except the direct excitation of Sm^{3+} ions. Upon excitation at 404 nm, the $La_{0.99}Sm_{0.01}MoBO_6$ phosphor shows an orange luminescence, and the obtained emission spectrum consists of f→f transition lines within Sm^{3+} $4f^5$ electron configuration, i.e., $^4G_{5/2} \rightarrow {}^6H_{5/2}$ (563 nm), $^4G_{5/2} \rightarrow {}^6H_{7/2}$ (597 nm), $^4G_{5/2} \rightarrow {}^6H_{9/2}$ (645 nm), and $^4G_{5/2} \rightarrow {}^6H_{11/2}$ (708 nm), respectively. The strongest one is located at 597 nm, corresponding to the $^4G_{5/2} \rightarrow {}^6H_{7/2}$ transition of Sm^{3+}. However, the quantum efficiency of 404-nm excited luminescence of $La_{0.99}Sm_{0.01}MoBO_6$ is only 15%.

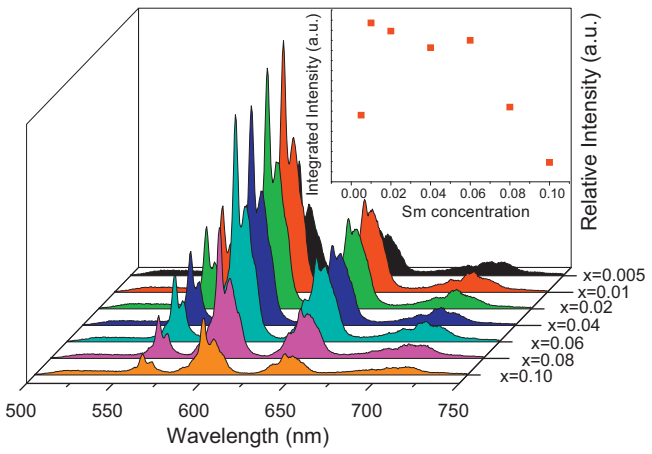

Fig. 3. Sm^{3+} concentration dependence on emission intensity of $La_{1-x}MoBO_6$:xSm^{3+} phosphors ($\lambda_{ex} = 404$ nm).

Fig. 3 shows the Sm^{3+} concentration dependence on emission intensity of $La_{1-x}Sm_xMoBO_6$ phosphors. It can be seen that the emission intensity increases with increasing Sm^{3+} concentration, and the maximum intensity approaches when the value of x is equal to 0.01, then the PL intensity decreases because of concentration quenching. The critical distance (R_0) from the concentration quenching data can be calculated using the following formula [23]

$$R_0 \approx 2 \times \left(\frac{3V}{4\pi x_C N}\right)^{1/3} \quad (1)$$

where x_c is the critical concentration at which the quenching occurs, N is the number of La^{3+} ions in the $LaMoBO_6$ unit cell, and V is the volume of the unit cell. By taking the experimental and analytic values of x_c, N and V (0.01, 8, 924.24 Å^3, respectively), the critical transfer distance of Sm^{3+} in $La_{1-x}Sm_xMoBO_6$ phosphors is determined to be about 28 Å.

3.3. Luminescence properties of $LaMoBO_6$ doped with Dy^{3+}

The excitation spectrum of $La_{0.995}Dy_{0.005}MoBO_6$ phosphor is shown in Fig. 4(a). The excitation bands at 353, 366, 389, 427 and 452 nm are assigned to the electronic transitions of $^6H_{15/2} \rightarrow (^4M,{}^4I)_{15/2}$, $^4I_{11/2}$, $^4I_{13/2}$, $^4G_{11/2}$ and $^4I_{15/2}$, respectively due to f→f transitions of Dy^{3+} [15]. Among them the intensity of $^6H_{15/2} \rightarrow {}^4I_{15/2}$ transition at 452 nm is the most intense one. In addition, it is interesting to note from Fig. 4(b) that for each sample the intensity of $^6H_{15/2} \rightarrow {}^4I_{13/2}$ transition become stronger than that of $^6H_{15/2} \rightarrow {}^4I_{15/2}$ transition with increasing Dy^{3+} concentration. Like in the previous case, the host related or $O^{2-} \rightarrow Dy^{3+}$ CT band has not been observed in the short wavelength range.

The emission spectrum of $La_{0.995}Dy_{0.005}MoBO_6$ ($\lambda_{ex} = 388$ nm) is shown in Fig. 5(a). Two emission bands are observed. The yel-

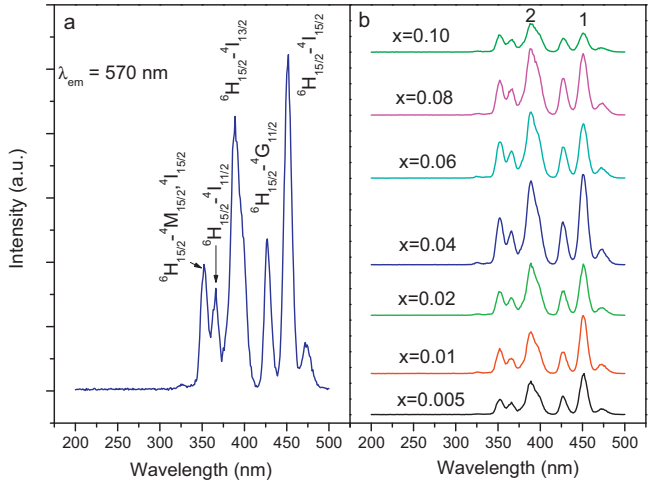

Fig. 4. PL excitation spectra of $La_{0.995}MoBO_6$:0.005Dy^{3+} (a) and $La_{1-x}MoBO_6$:xDy^{3+} (b).

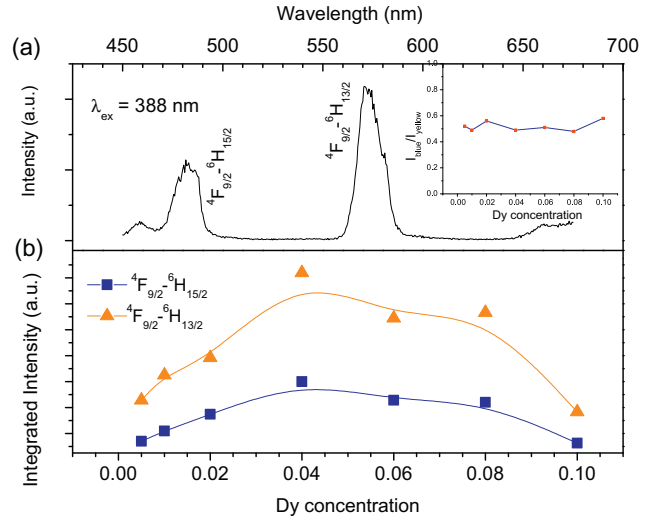

Fig. 5. PL emission spectra of $La_{0.995}MoBO_6$:0.005Dy^{3+} (a), the relationship between emission intensity and Dy^{3+} dopant contents (b). (the inset shows the ratio of B/Y with different Dy^{3+} contents).

low band (570 nm) corresponds to the hypersensitive transition $^4F_{9/2} \rightarrow {}^6H_{13/2}$ ($\Delta L = 2$, $\Delta J = 2$), and the blue band (482 nm) corresponds to the $^4F_{9/2} \rightarrow {}^6H_{15/2}$ transition. The value of B/Y (~0.5) does not vary much with increasing Dy^{3+} content (shown in the inset of Fig. 5(a)), which is consistent with other Dy^{3+} doped luminescent materials [13]. The Dy^{3+} content dependences on the emission intensity of $^4F_{9/2} \rightarrow {}^6H_{15/2}$ and $^4F_{9/2} \rightarrow {}^6H_{13/2}$ transitions are shown in Fig. 5(b). Both of them show similar tendency with increasing Dy^{3+} content. The optimum Dy^{3+} concentration is 4 mol%. However, the intensity is not strong, and the quantum efficiency of 452-nm excited luminescence of $La_{0.96}Dy_{0.04}MoBO_6$ is only 10%. The critical distance (R_0) calculated from Eq. (1) is about 18 Å.

3.4. Fluorescence decay spectra

The luminescence decay curves of the emission transition $^4G_{5/2} \rightarrow {}^6H_{7/2}$ at 597 nm (Sm^{3+} in $La_{1-x}Sm_xMoBO_6$) and that of the emission transition $^4F_{9/2} \rightarrow {}^6H_{13/2}$ at 570 nm (Dy^{3+} in $La_{1-x}Dy_xMoBO_6$) with a laser excitation at 355 nm are shown in Fig. 6(a) and (b), respectively. It can be seen that the decay curves are single exponential in the diluted samples. The luminescence lifetimes calculated from the fitted curves are 1.33 ms for Sm^{3+} in $La_{0.995}Sm_{0.005}MoBO_6$ and 0.53 ms for Dy^{3+} in $La_{0.995}Dy_{0.005}MoBO_6$. As concentration increases, the decay curves deviate from exponential behavior, and the non-exponential change becomes more prominent with increasing Sm^{3+} and Dy^{3+} content. Such decay curves are characteristic of quenching by direct transfer [24,25]. Since samples with low (Sm^{3+}, Dy^{3+}) content would minimize the effects of the interactions between optically active ions, the decay curves are nearly single exponential with a long lifetime. With increasing RE ions concentration, the distance between RE ions shortens; subsequently, the energy transfer between RE ions becomes more frequent, which provides an extra decay channel to change the decay curves, resulting in a non-exponential decay curve. The possible explanation for this luminescence quenching is due to the cross-relaxation by means of direct transfer between two ions. Cross-relaxation occurs easily between two neighboring rare-earth ions. This is the process whereby excitation energy from an ion decaying from a highly excited state promotes a nearby ion from the ground state to the metastable level [26]. For Sm^{3+} ion, the energy gap between the $^4G_{5/2}$ and $^6F_{9/2}$ levels is close to that between the $^6H_{5/2}$ and $^6F_{9/2}$ levels. The cross-relaxation channel in the $La_{1-x}Sm_xMoBO_6$ phosphors is $^4G_{5/2} + {}^6H_{5/2} \rightarrow {}^6F_{9/2} + {}^6F_{9/2}$ [25]. In the case of Dy^{3+} ion, the energy of the $^4F_{9/2} \rightarrow {}^6H_{5/2}$ transition matches that of the $^6H_{15/2} \rightarrow {}^6H_{5/2}$ transition. The cross-relaxation channel in the $La_{1-x}Dy_xMoBO_6$ phosphors is $^4F_{9/2} + {}^6H_{15/2} \rightarrow {}^6H_{5/2} + {}^6H_{5/2}$ [25].

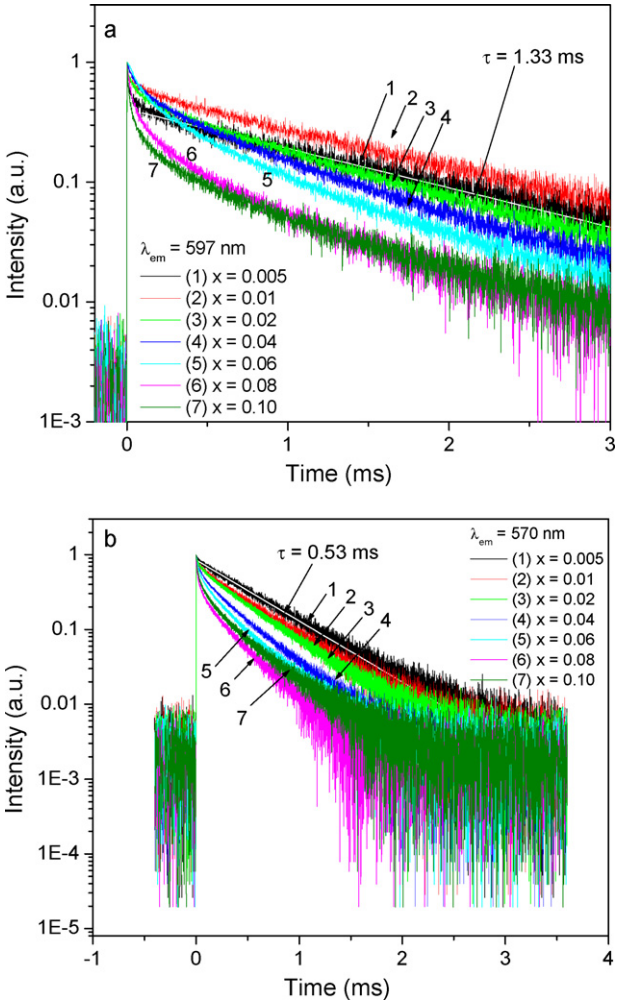

Fig. 6. Decay curves of $^4G_{5/2} \rightarrow {}^6H_{7/2}$ transition for Sm^{3+} in $La_{1-x}MoBO_6$:xSm^{3+} (a), and that of $^4F_{9/2} \rightarrow {}^6H_{13/2}$ transition for Dy^{3+} in $La_{1-x}MoBO_6$:xDy^{3+} (b).

4. Conclusions

The luminescence properties of Sm^{3+}, Dy^{3+} in the compound $LaMoBO_6$ are reported. $LaMoBO_6$:Sm^{3+} exhibits orange emission corresponding to the $^4G_{5/2} \rightarrow {}^6H_{7/2}$ transition. The emission spectrum of $LaMoBO_6$:Dy^{3+} exhibits two emission bands. The yellow band (570 nm) corresponds to the $^4F_{9/2} \rightarrow {}^6H_{13/2}$ transition, and the blue band (482 nm) corresponds to the $^4F_{9/2} \rightarrow {}^6H_{15/2}$ transition. The optimum concentrations are 1 mol% for Sm^{3+} and 4 mol% for Dy^{3+}. However, the intensity of Sm^{3+} and Dy^{3+} emission is not strong. The quantum efficiency is only 15% for $La_{0.99}Sm_{0.01}MoBO_6$ and 10% for $La_{0.96}Dy_{0.04}MoBO_6$. The decay curves are single exponential in the diluted samples, and the fitted lifetime is in the order of minisecond. The decay curves deviate from exponential behavior, and the non-exponential change becomes more prominent with increasing RE ions content. Cross-relaxation is responsible for the concentration quenching.

Acknowledgements

This work was supported by Mid-career Researcher Program through NRF grant funded by the MEST (No. 2009-0078682). This work was also supported by Science and Technology Program of Hunan Province (No. 2010FJ3092).

References

[1] I.M. Nagpure, K.N. Shinde, Vinay Kumar, O.M. Ntwaeaborwa, S.J. Dhoble, H.C. Swart, J. Alloys Compd. 492 (2010) 384–388.
[2] H. Yokota, M. Yoshida, H. Ishibashi, T. Yano, H. Yamamoto, S. Kikkawa, J. Alloys Compd. 495 (2010) 162–166.
[3] L. Zhou, J. Huang, F. Gong, Y. Lan, Z. Tong, J. Sun, J. Alloys Compd. 495 (2010) 268–271.
[4] X.M. Zhang, X.B. Qiao, H.J. Seo, J. Electrochem. Soc. 157 (2010) J267–J269.
[5] M.A.K. Elfayoumi, M. Farouk, M.G. Brik, M.M. Elokr, J. Alloys Compd. 492 (2010) 714–716.
[6] X.W. Zhu, Y. Masubuchi, T. Motohashi, S. Kikkawa, J. Alloys Compd. 489 (2010) 157–161.
[7] X.M. Zhang, H.J. Seo, J. Alloys Compd. 503 (2010) L14–L17.
[8] S.S. Yao, Y.Y. Li, L.H. Xue, Y.W. Yan, J. Alloys Compd. 491 (2010) 264–267.
[9] K. Shioi, N. Hirosaki, R.-J. Xie, T. Takeda, Y.Q. Li, J. Alloys Compd. 504 (2010) 579–584.
[10] Z. Xia, D. Chen, J. Am. Ceram. Soc. 93 (2010) 1397–1401.
[11] P. Li, Z. Wang, Z. Yang, Q. Guo, X. Li, J. Lumin. 130 (2010) 222–225.
[12] E. Cavalli, A. Belletti, R. Mahiou, P. Boutinaud, J. Lumin. 130 (2010) 733–736.
[13] Q. Su, Z. Pei, L. Chi, H. Zhang, Z. Zhang, F. Zou, J. Alloys Compd. 192 (1993) 25–27.
[14] I.M. Nagpure, V.B. Pawade, S.J. Dhoble, Luminescence 25 (2010) 9–13.
[15] G.S.R. Raju, S. Buddhudu, Spectrochim. Acta A: Mol. Biomol. Spectroc. 70 (2008) 601–605.
[16] Z. Lin, X. Han, C. Zaldo, J. Alloys Compd. 492 (2010) 77–82.
[17] S.-F. Wang, K.K. Rao, Y.-R. Wang, Y.-F. Hsu, S.-H. Chen, Y.-C. Lu, J. Am. Ceram. Soc. 92 (2009) 1732–1738.
[18] M. Thomas, P.P. Rao, M. Deepa, M.R. Chandran, P. Koshy, J. Solid State Chem. 182 (2009) 203–207.
[19] M.M. Haque, H.-I. Lee, D.-K. Kim, J. Alloys Compd. 481 (2009) 792–796.
[20] X. He, J. Zhou, N. Lian, J. Sun, M. Guan, J. Lumin. 130 (2010) 743–747.
[21] D. Zhao, W.D. Cheng, H. Zhang, S.P. Hang, M. Fang, Dalton Trans. (2008) 3709–3714.
[22] R.D. Shannon, Acta Crystallogr. Sec. A: Cryst. Phys. Diffr. Theor. Gen. Crystallogr. 32 (1976) 751–767.
[23] G. Blasse, Philips Res. Rep. 24 (1969) 131–144.
[24] B.e.R.K.W. Di Bartolo, Optical Properties of Ions in Solids, Plenum Publishing Corporation, New York, 1975.
[25] P. Kellendonk, G. Blasse, Phys. Status Solidi (b) 108 (1981) 541–548.
[26] Y.C. Li, Y.H. Chang, Y.F. Lin, Y.S. Chang, Y.J. Lin, J. Alloys Compd. 439 (2007) 367–375.